RSC Advances

PAPER

View Article Online
View Journal | View Issue

Cite this: *RSC Adv.*, 2025, **15**, 29490

Production of a bio-based liquid fuel additive, γ-valerolactone, over Ni-exchanged 12-tungstophosphoric acid anchored to zeolite HY using a biomass-derived H_2 source

Anjali Patel * and Kavan Chauhan

In present scenario the synthesis of sustainable biofuel additive using hydrogenation of biomass derived compound with green hydrogen source gained tremendous attention due to the fast-growing attention on the circular economy. So, in this work, we demonstrated the liquid phase hydrogenation of levulinic acid to γ-valerolactone using biomass derived green hydrogen source over a non-noble metal based heterogenous catalyst. Here, a non-noble metal-based catalyst, comprising nickel exchanged 12-tungstophosphoric acid anchored Zeolite HY, was synthesized and thoroughly characterized using various techniques, including EDS, NH_3-TPD, BET, FTIR, UV-vis-NIR, XPS, and HRTEM. In catalytic study it demonstrated outstanding performance, as obtained 72% yield of GVL, and 514 turnover number (TON). These confirmed the innovative strategy of eliminating the need for an external hydrogen source. These results emphasize the catalysts efficiency, superior activity, and stability under mild reaction conditions, make it as a more sustainable and effective alternative to existing non noble metal-based catalysts. Also, kinetic studies were conducted to determine the reaction order. Additionally, the in-situ reduction of Ni(II) to Ni(0), was studied and confirmed via XPS analysis. This work demonstrate the potential of catalyst in sustainable and renewable energy solutions, contributing significantly to the development of green and economically viable processes.

Received 8th July 2025
Accepted 7th August 2025

DOI: 10.1039/d5ra04872a

rsc.li/rsc-advances

Introduction

The hydrogenation reaction is one of the most essential and extensively used processes in the field of modern chemical industry and has a potential role in synthesizing a variety of chemicals and pharmaceutical intermediates.[1–4] Its wide range of usability make it significant industrial relevance is attributed to its wide usability range. However, it is highly challenging to perform because of the high-pressure hydrogen gas needed and several concerns such as the problem of storage and transportation. These above-mentioned problems cause difficulties in advancing the catalytic process and controlling the selectivity of the desired products. These limitations highlight the need for advancements in catalytic systems to make this processes safe, efficient, and environmentally benign. Towards the same aim, catalytic transfer hydrogenation (CTH) has gained significant attention as it offers multiple advantages compared to traditional methods such as eliminating the need for high-pressure hydrogen, safety risks and improved selectivity of the desired product due to the availability of different liquid hydrogen donors.[5–12]

Recently, the selective CTH of biomass-derived bioplatform molecules has gained tremendous attention and is considered a hot topic as the reaction products are directly used in various industries and biorefinery processes. In recent years, Pd, Pt, and Au noble metal-based catalysts were used for hydrogenation due to their good activity.[13–16] However, their large-scale application is significantly constrained in terms of economic considerations, including high costs and the limited availability of these resources. These factors drive the urgent need for developing cost-effective and sustainable alternatives using non-noble metals for greater affordability with the aim of sustainable production of biofuel additives from biomass-derived substrates.[17–21]

In this context, non-noble Ni-based heterogeneous catalysts are compatible for liquid phase hydrogenation. Their exceptional ability to drive these transformations and their tuneable and selective reactivity have established them as a foundation of catalytic innovation in both academic and industrial applications. Ni has been widely used in industrial chemical processes as it stands out as an affordable alternative compared to precious metals, offering significant advantages such as inherent Lewis acidity and exceptional compatibility with CTH.

Polyoxometalates and Catalysis Laboratory, Department of Chemistry, Faculty of Science, The Maharaja Sayajirao University of Baroda, Vadodara- 390020, Gujarat, India. E-mail: anjali.patel-chem@msubaroda.ac.in

These properties make Ni a promising candidate for developing cost-effective and efficient catalytic systems.[22–24]

From 2014 to 2025, notable advancements were made in nickel-based catalytic systems for the hydrogenation of levulinic acid (LA) to γ-valerolactone (GVL), showcasing improvements in the efficiency, selectivity, and reaction conditions. So, in 2014, Rode *et al.* developed an Ag–Ni/ZrO_2 nanocomposite catalyst, achieving 99% selectivity for GVL at 200 °C within 7 h.[25] In the same year, Chang *et al.* reported a Ni(20)Cu(60)-SiO_2 catalyst, delivering 92% selectivity at 265 °C.[26] After two years, in 2016, Kamaraju *et al.* demonstrated the gas-phase hydrogenation of LA using a Ni-based catalyst, achieving 77% GVL selectivity at 250 °C.[27] Concurrently, Varkolu *et al.* reported 93% LA conversion with a Ni/SiO_2 catalyst under similar conditions.[28] Furthermore, in 2017, Srinivasan *et al.* introduced an innovative approach involving the *in situ* formation of Ni(0), achieving nearly 100% GVL selectivity at 200 °C with the use of external molecular hydrogen.[29] Again, in the next year 2018, Srinivasan *et al.* further developed a Ni/SiO_2–Al_2O_3 catalytic system, achieving 70% LA conversion at 200 °C, over 10 h.[30] In 2019, Osawa *et al.* reported an efficient Ni/ZrO_2 catalyst, achieving an 86% GVL yield.[31] During the next year in 2020, de Souza *et al.* demonstrated a Ni-supported carbon nanotube catalyst that achieved 93% GVL selectivity at 180 °C under 30 bar pressure.[32] In the same year, Solsona *et al.* utilized natural clay-supported Ni, yielding 5.39% GVL at 180 °C.[33] After that, in the year 2022, Patel *et al.* pioneered the use of Ni-exchanged phosphomolybdic acid supported on ZrO_2, achieving 100% GVL selectivity at 200 °C within 6 h.[34] In 2024, Yan *et al.* demonstrated a zirconium phosphate-pillared zeolite MCM-36 catalyst, achieving 89.6% yield of GVL after 8 hours of reaction.[35] Also, Bae *et al.* reported on the catalytic performance of mesoporous silica, obtaining a 61% yield of GVL with 0.25 g of catalyst,[36] and Wu *et al.* showcased a CuNi alloy catalyst, delivering an 82% GVL yield under high-pressure conditions (6.5 MPa H_2) at 250 °C.[37] Akula *et al.* explored the use of a Ni-ZSM-5 catalyst, achieving 70% LA conversion with 61.8% GVL selectivity at 300 °C by taking 0.1 g of catalyst.[38] Recently, in 2025, Guo *et al.* developed a graphene-supported catalyst, Ni@FLG-600, which delivered a 68.2% yield of GVL under 5 bar H_2 pressure.[24]

The reported Ni-based catalysts require a large quantity of Ni and complex activation steps, including high temperature and pressure. To address these challenges, it is necessary to develop a new system that enables the *in situ* reduction of Ni(II) during the reaction, eliminating the need for a catalyst pretreatment step. Generated Ni(0) requires a stabilizing material that maintains Ni in its zero-oxidation state throughout the reaction, ensuring sustained catalytic activity. Recently, our group reported on the cascade upgrading of furfural using stabilized Ni-exchanged 12-tungstophosphoric acid ($H_3PW_{12}O_{40}\cdot xH_2O$) anchored zeolite HY (Ni-PW_{12}/ZHY).[22] 12-Tungstophosphoric acid (PW_{12}) has various proprieties such as a robust oxoanionic framework, tuneable redox properties, negative surface charge, and encapsulation capability, preventing aggregation and sintering.[22,23,39] Their structural integrity under reaction conditions enhances the catalytic performance. These features make them ideal for stabilizing Ni nanoparticles in catalytic applications.

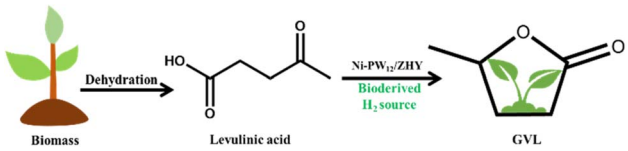

Scheme 1 Liquid phase hydrogenation of biomass-derived levulinic acid to γ-valerolactone (GVL).

These excellent properties of PW_{12} inspired us to further expand this study for the hydrogenation of levulinic acid (LA – *The sleeping giant of the biorefinery world – born from waste, destined for future worth*) to GVL using a bioderived hydrogen source (Scheme 1). The use of formic acid (FA) is also a green and safe approach, as it is a by-product of LA when hexoses are dehydrated in biorefineries. FA has emerged as an important bioderived chemical for hydrogen storage, as it possesses a high hydrogen content and is nontoxic in nature. The produced GVL is a promising platform bioproduct, offering potential precursors to make value-added chemicals, including gasoline-range and liquid hydrocarbon fuels.[40,41] This method has emerged as a sustainable and applicable approach in the field of green chemistry.

Experimental

Materials

All chemicals used were of A. R. grade and were used as received from Merck, including 12-tungstophosphoric acid (extra pure), nickel acetate, levulinic acid (99%), ammonium chloride (99%), and formic acid (>98%), while zeolite NaY was commercially obtained from Reliance Industries Limited, Vadodara, Gujarat.

Synthesis of the catalyst

Treatment of zeolite NaY to convert into zeolite HY (ZHY). The Na form of zeolite was converted into its H (protonic) form *via* an ion exchange method (Scheme 2), as described earlier.[42] Zeolite NaY was refluxed with 1 M NH_4Cl solution for 2 h at 80 °C. After that, it was filtered, washed with double distilled water, and dried for 4 h at 120 °C in a hot oven. The process was repeated twice to ensure complete ion exchange. Finally, the obtained material was calcined at 550 °C for 5 h to obtain the protonic form ZHY.

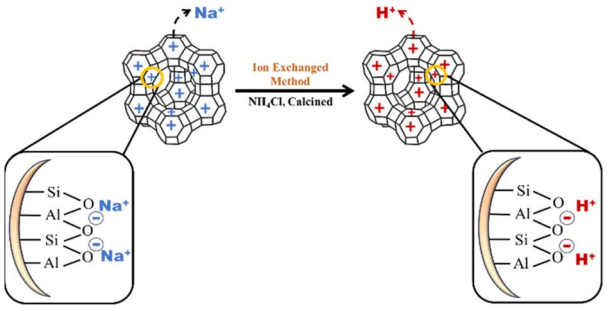

Scheme 2 Ion Exchange Method to convert zeolite NaY into Zeolite HY.

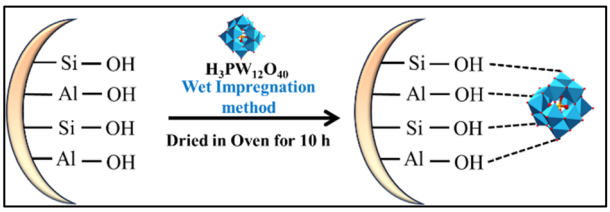

Scheme 3 Synthesis of PW_{12}/ZHY by the wet impregnation method.

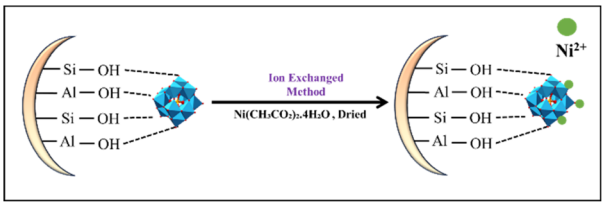

Scheme 4 Synthesis of Ni-PW_{12}/ZHY by the ion exchange method.

Synthesis of 12-tungstophosphoric acid anchored into ZHY (PW_{12}/ZHY). PW_{12}/ZHY was synthesized by incipient wet impregnation method (Scheme 3), as reported earlier by our group.[22,42] 1 g of zeolite HY was impregnated with an aqueous solution of (12-tungstophosphoric acid) PW_{12} (0.3 g/30 mL) in double-distilled water. The mixture was stirred for 5 h and subsequently dried for 10 h at 100 °C to evaporation of suspension water. Finally, the synthesized material PW_{12}/ZHY was obtained.

Synthesis of non-noble metal Ni exchanged PW_{12}/ZHY (Ni-PW_{12}/ZHY). The synthesis of Ni-PW_{12}/ZHY was achieved by exchanging the Ni with the available counter protons of PW_{12} in PW_{12}/ZHY (Scheme 4), as described earlier by our group.[22,34] For that, 1 g of PW_{12}/ZHY was soaked in 25 mL of 0.04 M aqueous solution of nickel acetate with interval stirring for 24 h at room temperature (R.T.). After that, the solution was filtered, washed with double-distilled water to remove excess Ni, and air-dried. The obtained greenish color material was designated as Ni-PW_{12}/ZHY.

Characterization techniques

A comprehensive characterization of Ni-PW_{12}/ZHY has been previously reported in our earlier work.[22] In this study, elemental analysis (EDS), acidity measurement using NH_3-TPD, BET surface area analysis, FT-IR and XPS were discussed for the reader's convenience. Additionally, HRTEM imaging and a particle size histogram have been included.

Acidity measurements

NH_3-TPD. The NH_3 temperature-programmed desorption (NH_3-TPD) was conducted using the BELCAT-II equipment manufactured by MicrotracBEL Corp. (Japan). In the presence of a pure helium gas mixture (99.9%, flowing at a rate of 30 mL per minute), a dry catalyst weighing 0.05 g was loaded and subjected to a pre-treatment process at a temperature of 300 °C for a duration of 1 hour. A 10% NH_3 in He gas mixture was used to adsorb ammonia onto the surface of the substance for a duration of 1 hour. Subsequently, the physisorbed ammonia was eliminated by flushing the material with pure He gas. The temperature programming procedure comprised a gradual increase in temperature from 100 to 600 °C, with a rate of 10 °C per minute. The emitted NH_3 was then monitored using a thermal conductivity detector (TCD) incorporated in the experimental setup.

Physiochemical techniques

The nickel content was quantified through volumetric analysis by using a titration method, and measuring the differences between the standard solution and the sample solution.[22,23]

The JSM-7600F microscope was equipped with attachment systems for energy-dispersive X-ray spectroscopy (EDS) and scanning transmission electron microscopy (STEM). A PerkinElmer NexION 2000 apparatus was used for inductively coupled plasma mass spectrometry (ICP-MS) analysis, and the solid catalyst samples (fresh and used) were digested using microwave-assisted acid digestion with a Titan MPS, PerkinElmer. The BET (Brunauer–Emmett–Teller) surface area measurements were performed using a Micromeritics ASAP 2010 (USA) volumetric static adsorption instrument with N_2 physisorption at 77 K, and the calculations of the pore size distributions were done using the BJH adsorption–desorption method. FTIR analysis was done using KBr wafer on a Shimadzu instrument (IRAffinity-1S). UV-Vis-NIR spectra were recorded using a JASCO V-770 instrument. X-ray photoelectron spectroscopy (XPS) measurements were recorded by using an Auger electron spectroscopy (AES) module PHI 5000 Versa Prob II. The high-resolution transmission electron microscopy (HRTEM) analysis was conducted using a field emission gun-transmission electron microscope (resolution: point: 0.19 nm, line: 0.1 nm, magnification: 50–1.5 M× accelerating voltage of 200 kV; Make: JEOL; Model: JEM 2100F).

Assessment of catalytic activity

The hydrogenation of LA was performed following the same method reported by our group.[34] LA and FA were charged into a Teflon-lined stainless-steel autoclave, and subsequently sealed and placed in an oven at the desired temperature and time. After the reaction completion, the product was extracted using a dichloromethane solvent, and the catalyst was separated from the junction between the organic and liquid phase, followed by centrifugation. Anhydrous $MgSO_4$ was used to dry the organic phase, and was identified by gas chromatography and gas chromatography-mass spectrometry (GC-MS) using a Shimadzu GC-2010 Plus system fitted with a ZB-5 MSi column (30 m length, 0.25 mm internal diameter).

Result and discussion

The nickel content in the synthesized catalyst was quantified as 1.64 wt% through volumetric titration analysis.[22] Additionally, energy-dispersive X-ray spectroscopy (EDS) analysis was performed to determine the wt% of nickel in the synthesized

catalyst. The results revealed a Ni content of 1.60 wt%, which closely matches the calculated theoretical value of 1.64 wt%. Additionally, ICP-MS analysis exhibited 1.63 wt% of Ni in the synthesized catalyst. This excellent agreement confirms that the desired amount of Ni was successfully exchanged with the available counter cations of PW_{12} during the catalyst synthesis.

The Lewis acidic strength of the synthesized catalyst was measured from the ammonia TPD analysis. PW_{12}/ZHY exhibits 0.748 mmol g^{-1} for weak acidity. In comparison, Ni-PW_{12}/ZHY shows 0.897 mmol g^{-1} for weak acidity, *i.e.*, Lewis acidity, which was due to the nickel (Table S1). This confirms that the required Lewis acidity was present in the synthesized catalyst.[22,43–45]

To characterize the textural properties of the synthesized catalysts, BET surface area analysis was performed. Ni-PW_{12}/ZHY (Table S2) revealed a notable decrease in both total surface area and pore volume compared to PW_{12}/ZHY. This reduction is attributed to the successful exchange of Ni with the available protons (counter cation) of PW_{12}. The N_2 adsorption–desorption isotherm of PW_{12}/ZHY (Fig. S1a) exhibits a Type-I isotherm with an H1 hysteresis loop, which is characteristic of microporous materials.[46,47] As expected, the type of isotherm for Ni-PW_{12}/ZHY (Fig. S1b) remained unchanged even after Ni exchange, confirming the preservation of the structural property characteristics of PW_{12}/ZHY.[22]

The FTIR spectra of ZHY, PW_{12}, PW_{12}/ZHY, and Ni-PW_{12}/ZHY are depicted in Fig. S2. ZHY exhibits characteristic bands at 1145 cm^{-1} (Si–O(Si)) and 1057 cm^{-1} (Si–O(Al)), which correspond to the asymmetric stretching in SiO_4 and AlO_4 tetrahedra. PW_{12}/ZHY retains the Keggin structure of PW_{12}, with bands at 1080 cm^{-1} (P═O stretching) and 897 cm^{-1} (W–O–W asymmetric stretching).[42,47] In Ni-PW_{12}/ZHY, all PW_{12} bands are present but shifted, which is likely due to Ni exchange with PW_{12} protons. Additional bands are absent, possibly due to overlap with ZHY bands at 982 cm^{-1} and 821 cm^{-1}.[22]

The high-resolution XPS spectra of Ni-PW_{12}/ZHY (Fig. 1) show a faint peak at 854.3 eV, corresponding to the Ni $2p_{3/2}$ binding energy, confirming the presence of the Ni(+2) species. The low intensity is attributed to the minimal Ni content (1.6 wt%). A prominent peak at 530 eV corresponds to the O 1s orbital, indicating oxygen in the ZHY framework and PW_{12} structure. The XPS of W 4f shows peaks at 35.3 eV and 37.5 eV, which are assigned to W $4f_{7/2}$ and W $4f_{5/2}$, respectively, confirming tungsten in the +6-oxidation state of the synthesized catalyst.[48–50]

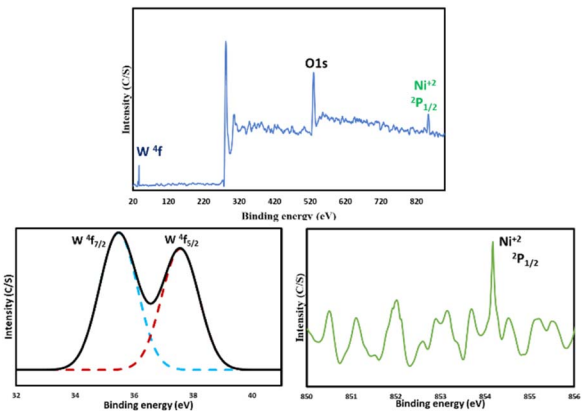

Fig. 1 XPS spectra of Ni-PW_{12}/ZHY.

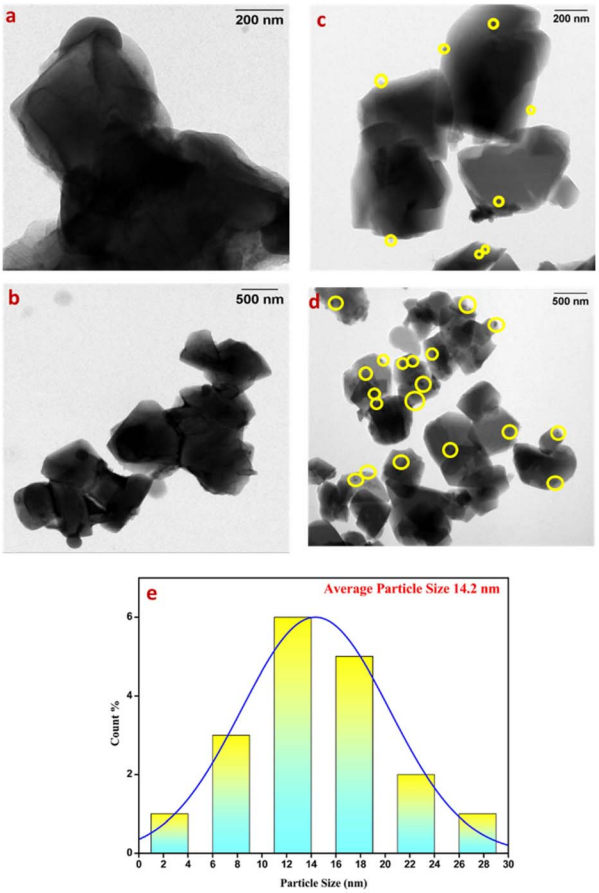

Fig. 2 HRTEM images of (a and b) PW_{12}/ZHY, (c and d) Ni-PW_{12}/ZHY and (e) particle size distribution for the catalyst.

Fig. 2 presents HRTEM images of PW_{12}/ZHY and Ni-PW_{12}/ZHY at various magnification levels. The HRTEM images of PW_{12}/ZHY (Fig. 2a and b) confirm the successful incorporation of the PW_{12} species within the hexagonal channels of ZHY, with the structural integrity of the material preserved.[51] Additionally, HRTEM images of Ni-PW_{12}/ZHY (Fig. 2c and d) clearly show that the hexagonal framework of ZHY remains intact, in agreement with the XRD analysis, which indicates no significant changes in the surface morphology even after the loading of the active species. The average Ni metal particle size was also determined from HRTEM as 14 ± 1.5 nm (Fig. 2e).[22,42]

Catalytic study

The catalytic performance of the synthesized Ni-PW_{12}/ZHY was evaluated for the liquid-phase hydrogenation of levulinic acid (LA), using a bioderived hydrogen source, formic acid (FA), as an *in situ* hydrogen source (Scheme 5). To achieve the optimum catalytic efficiency and maximize the % yield of the product, various reaction parameters such as the catalyst amount, molar ratio, temperature, and reaction time were thoroughly studied.

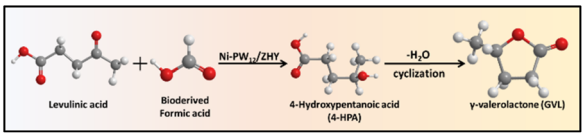

Scheme 5 Liquid phase hydrogenation of levulinic acid to GVL using a bioderived H_2 source.

Each experiment was conducted four times under optimized conditions to ensure its reproducibility, with the results showing a reliable margin of error within ±1.0–1.5%.

The hydrogenation reaction was carried out in a closed hydrothermal reactor using 50 mg catalyst, 5 mmol LA, and 125 mmol FA. After, the reactor was placed in a pre-heated oven at 200 °C for 6 h. After the completion of the reaction, the product γ-valerolactone (GVL) was extracted and analyzed using ^{1}H NMR, GC and GC-MS spectroscopy, as depicted in Fig. S3, S4 and S5, respectively.

The effect of the catalyst for the conversion of LA was evaluated by varying the catalyst amount, ranging from 10 mg to 60 mg, as showed in Fig. 3. The obtained results reveal that the conversion efficiency of LA to GVL improved with increased catalyst amounts. This enhancement is due to the greater accessibility of Ni active sites (1.4×10^{-2} mmol), which promote the breakdown of formic acid (FA), leading to greater conversion. Nonetheless, when the catalyst quantity was raised to 60 mg, the conversion rate showed only a slight increase (3%). So, based on the above explanation, 50 mg of catalyst was chosen for further optimization studies.

The effect of the bioderived hydrogen source, *i.e.*, formic acid (FA), was also studied by varying the molar ratio of FA from 1 : 10 to 1 : 30 mmol. As we can see from Fig. 3, by increasing the FA molar ratio from 50 to 125 mmol, a significant improvement is shown in the % conversion of LA from 23% to 72%.

The influence of the reaction time on achieving the maximum conversion was also investigated. As depicted in Fig. 3, the % conversion increases from 15% to 72% as the reaction time is extended from 2 h to 6 h. Subsequently, a reaction time of 6 h was selected as the optimal time for achieving the maximum conversion of LA.

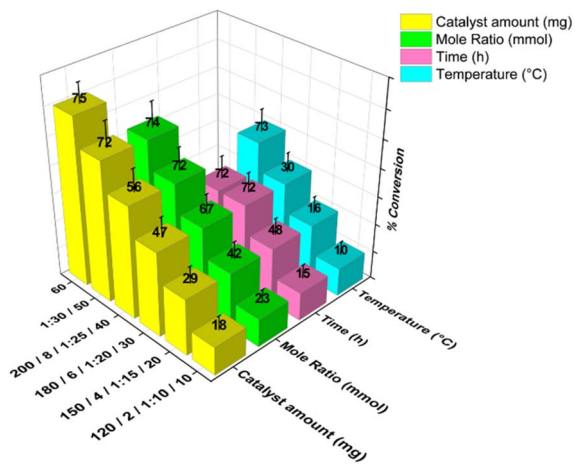

Fig. 3 Different reaction conditions for optimization of the hydrogenation of levulinic acid.

Furthermore, the effect of temperature on the reaction was also evaluated within the range of 120 to 200 °C. Fig. 3 shows that the % conversion was increased with increasing temperature. This trend can be attributed to the enhanced dissociation of formic acid (FA) into hydrogen at higher temperatures, forming *in situ* hydrogen that facilitated the conversion of LA to GVL. Therefore, a temperature of 200 °C was selected.

The optimized reaction conditions can be summarized as follows: firstly, the substrate-to-formic acid (FA) ratio was 1 : 25; the quantities of the reagents were 50 mg catalyst (containing 1.4×10^{-2} mmol of active Ni sites), 5.0 mmol of levulinic acid, and 125 mmol of FA; with 6 h reaction time, and 200 °C temperature. Under these optimized conditions, 72% conversion of levulinic acid was achieved, accompanied by a high turnover number (TON) of 514 and turnover frequency (TOF) of 86 h^{-1}. Additionally, the carbon balance for the reaction was determined to be 72% and 100% atom economy.

The promising outcomes achieved with the current catalytic performance encouraged us to further scale-up the reaction as GVL may have significant industrial relevance. In pursuit of this goal, the hydrogenation reaction was scaled by proportionately increasing the quantities of reactants (LA + FA) and the catalyst. We used 5 × the initial millimolar scale amounts of LA, formic acid (FA), and catalyst for scale-up in order to maintain consistency and avoid problems due to addition mode complexities.

Significantly, in this system, the catalyst exhibits exceptionally desirable performance. It can act at high substrate concentrations, with 72% conversion and 100% selectivity toward γ-valerolactone (GVL) under optimal conditions. This scalability is especially promising, as the catalyst maintains high activity when scaled to larger dimensions, a consideration that is relevant for possible industrial application.

Green metric

The green matrices for the said reaction are as follows. The environmental factor (E-factor) determines how much waste is generated during the chemical process. Lowering the number demonstrates a more environmentally friendly chemical reaction. In this particular reaction, the E-factor value is 1.24, which is less than 5, suggested an environmentally friendly reaction. Carbon efficiency known as the percentage of carbon atoms in the reactants that are effectively converted into the final product. It measures how well carbon is used in a chemical process. In this case, the carbon efficiency is 72%, which is good. There was also no solvent used in the reaction, so the value of the solvent intensity (SI) is zero.

Kinetic study: determination of the activation energy (E_a)

Kinetic studies were performed to study the order of the said hydrogenation reaction using the Ni-PW_{12}/ZHY catalyst. The experiments were performed between the temperature range of 180–220 °C for 2–8 h, confirming first-order kinetics (Fig. 4).[52,53]

Activation energy (E_a) is an important parameter particularly in the field of heterogeneous catalysis, as it provides insight into the efficiency of the interaction between reactants and the catalyst. Determining E_a is vital for understanding the fundamental chemical processes involved.[42] A linear relationship was observed in the plot of the natural logarithm of the rate constant, ln(k), *versus* the reciprocal of temperature, $1/T$ (Fig. 5). This relationship was used to calculate E_a using the Arrhenius equation, and obtained 55 kJ mol^{-1} supports that it is a true chemical reaction step.[54]

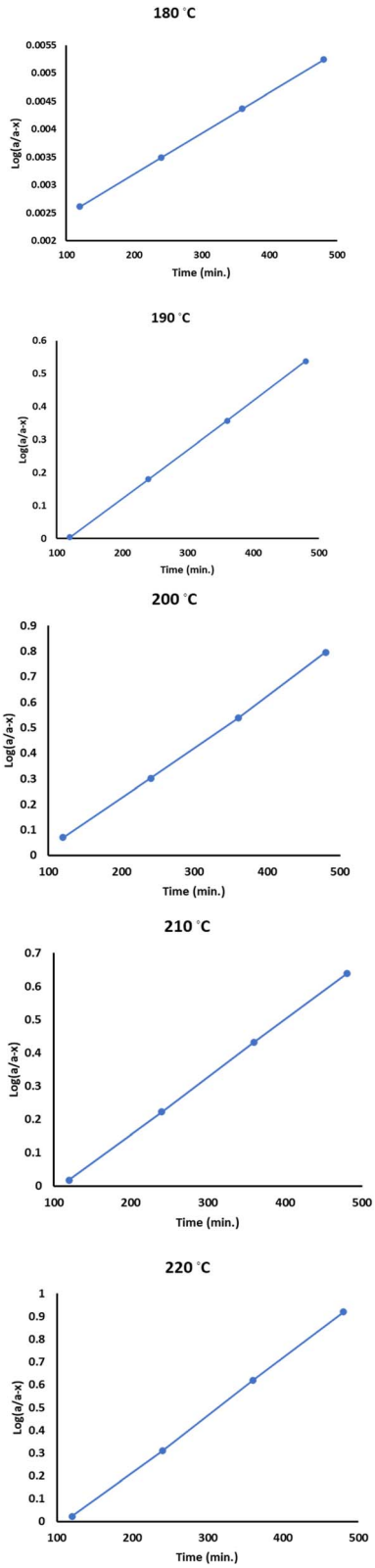

Fig. 4 Plots of log[$a/(a-x)$] *vs.* time.

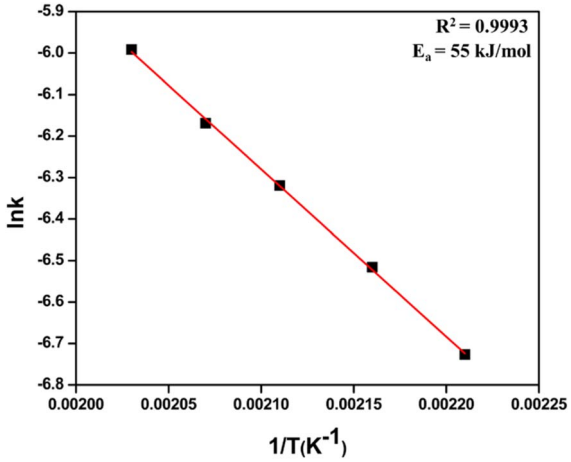

Fig. 5 Kinetics plot of ln k *vs.* $1/T$.

Control experiments

Control experiments were conducted under optimized conditions to evaluate the individual contributions for the CTH of LA. The results are summarized in Table 1. We can see that only Ni-containing materials can perform well for the said reaction, as it requires Lewis acidity. So, the activity of Ni/ZHY is notable compared to that of ZHY, indicating that the active component Ni plays a crucial role in this reaction.[34] PW_{12} alone does not achieve any conversion due to its Brønsted acidity, while ZHY exhibited 32% conversion. This is attributed to the presence of Si–O–Al and Si–O–Si groups within the zeolitic framework, which acts as Lewis acidic sites.[55,56] The Brønsted acidic PW_{12}/ZHY achieved a 41% conversion. This is 11% less compared to Ni/ZHY, as the Brønsted acidity hindered the reaction process. To confirm the activity of Ni, we performed the same reaction with $Ni(CH_3CO_2)_2$. It demonstrated 57% conversion of LA; hence, proving that the active component Ni plays a crucial role. However, its solubility in the reaction mixture posed challenges for separation. In contrast, Ni-PW_{12}/ZHY, which combines the Lewis acidic sites of nickel and is stabilized with the PW_{12}, achieved the highest conversion of 72% (with an isolated GVL yield exceeding 71.4%).

Hot filtration and heterogeneity test

In heterogeneous catalysis, the stability and reusability of a catalyst, including its ability to maintain active sites and heterogeneity over multiple cycles, are critical factors. To assess these properties, a hot filtration test was conducted to investigate potential nickel (Ni) leaching from the synthesized Ni-PW_{12}/ZHY catalyst under controlled reaction conditions. The reaction was initiated with the catalyst and allowed to proceed for 3 h (Fig. 6). The catalyst was then removed *via*

Table 1 Control experiment

Catalyst	% Conversion	% Selectivity
 [a]PW_{12}	—	—
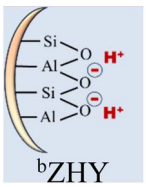 [b]ZHY	32	100
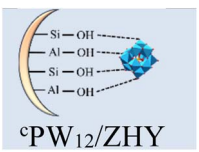 [c]PW_{12}/ZHY	41	100
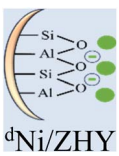 [d]Ni/ZHY	52	100
 [e]$Ni(CH_3CO_2)_2$	57	100
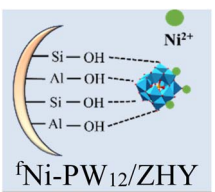 [f]Ni-PW_{12}/ZHY	72	100

Reaction conditions: catalyst ([a]11.4 mg, [b]38.46 mg, [c]49.2 mg, [d]50 mg, [e]0.8 mg, [f]50 mg), LA (5 mmol), FA (125 mmol), time (6 h) and temperature (200 °C).

centrifugation, and the reaction was continued for an additional 6 hours using the filtrate. After the reaction, the organic layer was extracted using dichloromethane and analyzed by gas chromatography. The consistent percentage conversion observed before and after catalyst removal confirmed the absence of Ni leaching. Furthermore, the reaction mixture was filtered post-reaction, and inductively coupled plasma (ICP) analysis was performed to detect any Ni presence. No Ni was detected in the reaction mixture. Additionally, ICP analysis of both fresh and recovered catalysts revealed a consistent Ni content of 0.82 mg, further confirming the stability and integrity of the catalyst.

Catalyst reusability

The durability and reusability of a catalyst are critical aspects of any catalytic process. After the reaction, the catalyst was

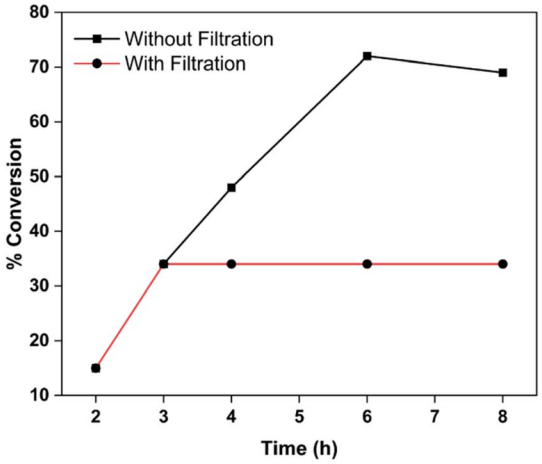

Fig. 6 Reaction conditions: catalyst (50 mg), LA (5 mmol), FA (125 mmol), time (6 h) and temperature (200 °C).

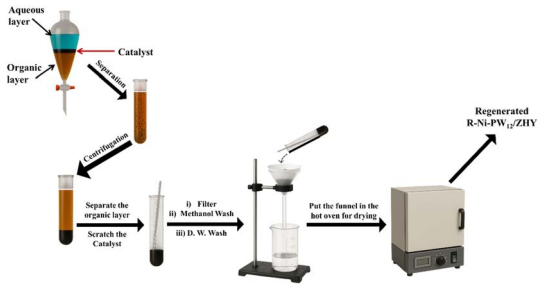

Scheme 6 Regeneration of the synthesized catalyst.

recovered *via* centrifugation, washed with methanol and water, and dried for reuse in subsequent cycles (Scheme 6).

As shown in Fig. 7, the percentage conversion of levulinic acid (LA) remained consistent over three consecutive runs, with only minimal variation. This observation underscores the catalyst's stability and confirms its truly heterogeneous nature. The catalyst demonstrated excellent catalytic activity and could be easily used for up to four cycles. Of course, the potential for further reuse depends on the individual requirements. These results highlight the robustness and durable performance of the synthesized catalyst, emphasizing its suitability for practical applications.

Characterization of the regenerated catalyst

To confirm the structural integrity and sustainability of the regenerated catalyst, R-Ni-PW_{12}/ZHY, two different characterization techniques (UV-Vis-NIR and XPS) were used.

The UV-Vis-NIR analysis of the regenerated catalyst (Fig. 8b) reveals characteristic peaks for nickel (Ni) in the ranges of 850–580 nm and 450–370 nm (Fig. 8). The broadening of the peak in the 365–375 nm range is likely attributed to the presence of Ni(0), a finding further corroborated by XPS analysis.[22,57] This observation confirms that nickel does not leach into the solution during the reaction process, highlighting the stability and durability of the catalyst. The consistent spectral features across

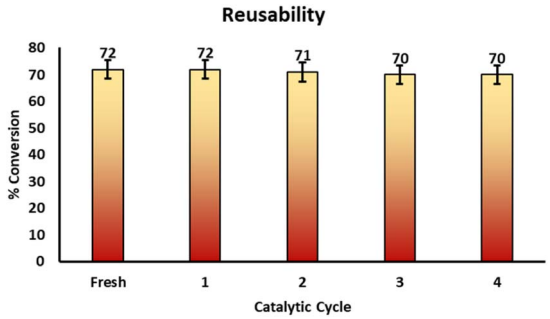

Fig. 7 Catalyst reusability under optimised conditions.

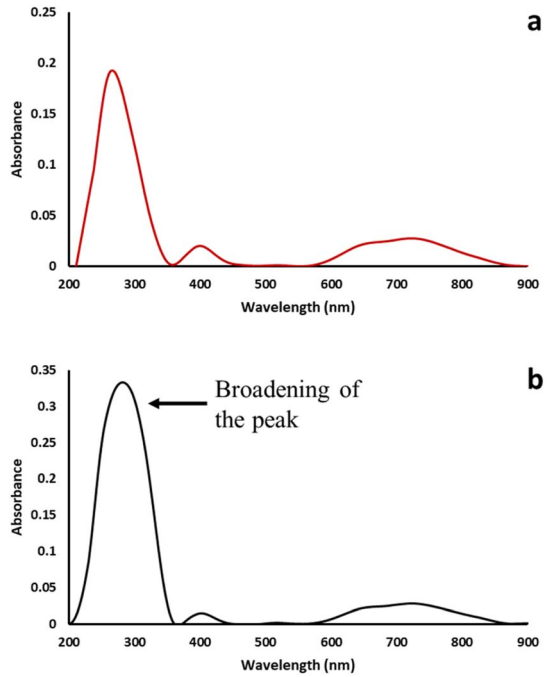

Fig. 8 UV-Vis-NIR spectra of (a) Ni-PW_{12}/ZHY and (b) R-Ni-PW_{12}/ZHY.

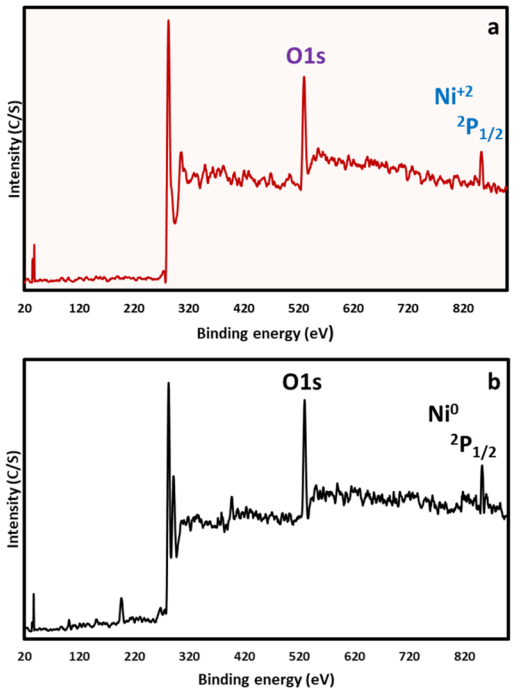

Fig. 9 XPS spectra of (a) Ni-PW_{12}/ZHY and (b) R-Ni-PW_{12}/ZHY.

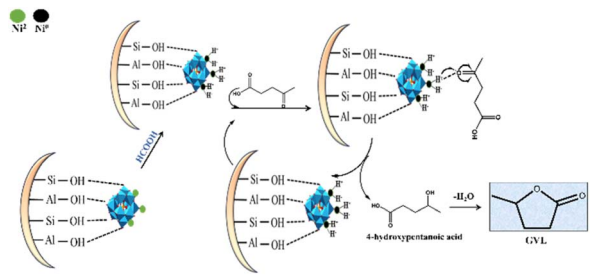

Fig. 10 Plausible reaction mechanism of LA hydrogenation over Ni-PW_{12}/ZHY.

regeneration cycles underscore the catalyst's ability to maintain its structural and functional integrity, reinforcing its suitability for repeated use in catalytic applications.

XPS analysis of the regenerated catalyst (Fig. 9) confirms the reduction of nickel from Ni^{2+} to Ni^0 during the reaction. However, the binding energy peak corresponding to Ni shifts from 853.3 eV to 852.2 eV, indicating the formation of Ni(0) during the reaction process.[58,59] This reduction of Ni^{2+} to Ni^0 further validates the catalyst's stability and structural integrity, as well as its ability to maintain active sites without leaching into the solution. These findings reinforce the durability and reusability of the catalyst in catalytic applications.

Reaction mechanism

The plausible reaction mechanism for Ni-PW_{12}/ZHY catalysed levulinic acid hydrogenation is shown in Fig. 10. Firstly, the adsorption of FA occurs onto the active nickel (Ni) sites of the catalyst, and dehydrogenation was occurred which was early published by our group.[34] This first step produces H_2 and CO_2, where H_2 reduces Ni(II) to Ni(0), while CO_2 remains inactive in the reaction. The resulting Ni(0) forms Ni–H_2 hydride complex (Fig. 10), which is available as the active site for the next steps. Further, LA adsorbs onto the Ni–H_2 site through the oxygen atom of its carbonyl group (C=O). The hydride from the Ni–H_2 complex, transferred to the carbonyl carbon of LA, leading to the formation of 4-hydroxypentanoic acid as an intermediate. This intermediate undergoes rapid intramolecular condensation, where the hydroxyl group reacts with the carboxyl group, resulting in the formation of γ-valerolactone (GVL) and release one molecule of water through dehydration step. Finally, GVL desorbs from the catalyst surface, regenerating the active sites for further catalytic cycles. This proposed mechanism aligns with experimental observations and highlights the catalyst efficiency, stability, and reusability. The reduction of Ni(II) to Ni(0) during the reaction, as confirmed by XPS analysis, further

supports the proposed pathway. The absence of leaching and the consistent performance of the catalyst over multiple cycles underscore its robust and heterogeneous nature, making it a promising candidate for sustainable catalytic applications.

Superiority over reported hydrogenation systems

The catalytic efficiency of the reported system is summarized in Table S3, specifically highlighting the reaction conditions of the hydrogenation of levulinic acid (LA). This table provides insights into GVL selectivity, along with essential reaction parameters, including hydrogen sources, solvents, reaction time, and temperature. After examination, it reveals that most catalysts (entries 1–7) required very harsh conditions, high catalyst loading, solvent usage, and elevated temperatures. Additionally, many of these catalysts depend on high-pressure molecular hydrogen (H_2) as the reductant, which presents challenges in terms of safety and handling. So, Ni-PW_{12}/ZHY demonstrates superior performance, achieving 100% selectivity only with entry 2 (NiAl-LDH), which requires high-pressure H_2 (40 bar). Conversely, in our case, we use bioderived formic acid (5 mmol) as a more secure hydrogen source. Entry 1 (Ni/MgO) and entry 3 (Ni/SiO_2) achieve 94% and 93% selectivity, respectively, but they operate under harsh conditions with respect to the reaction temperature (523 K) and reaction time (10 h) compared to our optimized conditions (473 K, 6 h).

Some systems have particularly substantial weaknesses. Entry 4 (Ni-PMo_{12}/ZrO_2) and entry 5 (Ni/CNT) both demonstrate low selectivity, despite the use of formic acid (47% selectivity) and pressurized H_2 (24% selectivity), respectively. Also, unlike entry 6 (2-propanol system, 86% selectivity), entry 7 (dioxane system, 90.2% selectivity) which rely on solvents, our solvent-free system features its advantages as we do not have to go through purification steps to handle the solvent.

The Ni-PW_{12}/ZHY catalyst shows exceptional activity and stability under optimized conditions. This is attributed to the 12-tungstophosphoric acid (PW_{12}) modification with Ni, positioning it as a cost-effective, scalable, and environmentally benign solution, superior to previously reported systems that compromise the selectivity and reaction complexity. More importantly, the catalyst explored in this study demonstrates exceptional efficiency, achieving 100% GVL selectivity under solvent-free conditions while operating with lower catalyst loading, a biomass derived green hydrogen source, and moderate optimized reaction conditions, surpassing previously reported catalytic systems.

Conclusion

The synthesized Ni-PW_{12}/ZHY shows excellent catalytic activity to produce GVL from LA under mild reaction conditions. The present approach effectively uses a bioderived hydrogen source instead of relying on an external hydrogen source. The main aspect of this research is the effective replacement of expensive precious metals with nickel using very low Ni loading (0.82 mg). This innovative approach provides a viable pathway for producing high-value fuel additives, contributing to the development of sustainable energy solutions. Through the direct transformation of renewable LA into GVL, a key biofuel additive, this study may establish a foundation for cost-effective and scalable biorefinery processes in the future.

Author contributions

Anjali Patel: conceptualization, validation, writing – review & editing, visualization, supervision. Kavan Chauhan: methodology, validation, formal analysis, investigation, writing – original draft.

Conflicts of interest

There are no conflicts to declare.

Data availability

All additional data to supporting this article are included in the manuscript and/or as part of the SI. See DOI: **https://doi.org/10.1039/d5ra04872a**.

Acknowledgements

AP and KC are thankful to the Gujarat Council on Science and Technology (GUJCOST), Gandhinagar, for financial support, Research Project Ref. No. (GUJCOST/STI/2021-22/3825). AP and KC are also thankful to the Department of Chemistry, The Maharaja Sayajirao University of Baroda for the infrastructural facilities and DST-FIST for BET surface area analysis.

References

1 S. Anand, D. Pinheiro and S. Devi, *Asian J. Org. Chem.*, 2021, **10**, 3068–3100.
2 M. Stoffels, F. Klauck, T. Hamadi, F. Glorius and J. Leker, *Adv. Synth. Catal.*, 2020, **362**, 1258–1274.
3 G. Filonenko, R. Putten, E. Hensen and E. Pidko, *Chem. Soc. Rev.*, 2018, **47**, 1459.
4 W. Gong, J. Ma, G. Chen, Y. Dai, R. Long, H. Zhao and Y. Xiong, *Chem. Soc. Rev.*, 2025, **54**, 960–982.
5 D. Sharma, P. Choudhary, P. Mittal, S. Kumar, A. Gouda and V. Krishnan, *ACS Catal.*, 2024, **14**, 4211–4248.
6 T. Toyao, S. M. A. Hakim Siddiki, K. Kon and K.-i. Shimizu, *Chem. Rec.*, 2018, **18**, 1374–1393.
7 K. Hengst, M. Schubert, H. W. P. Carvalho, C. Lu, W. Kleist and J.-D. Grunwaldt, *Appl. Catal., A*, 2015, **502**, 18–26.
8 X. Gu, X. Li, J. Xie and Q. Zhou, *Acta Chim. Sin.*, 2019, **77**, 598.
9 R. Qu, K. Junge and M. Beller, *Chem. Rev.*, 2023, **123**, 1103–1165.
10 P. Choudhary, A. Bahuguna, A. Kumar, S. S. Dhankhar, C. Nagaraja and V. Krishnan, *Green Chem.*, 2020, **22**, 5084–5095.
11 H. Qiu, J. Ren, L. Zhang, R. Song, W. Si, D. Yang, L. Wen and J. Lv, *Green Chem.*, 2023, **25**, 3948–3955.

12 Y. Wang, B. Chen, H. Wu, X. Mei, K. Zhang, B. Zheng, W. Han, J. Xu, M. He and B. Han, *Green Chem.*, 2023, **25**, 1835–1841.
13 L.-H. Gong, Y.-Y. Cai, X.-H. Li, Y.-N. Zhang, J. Su and J. S. Chen, *Green Chem.*, 2014, **16**, 3746–3751.
14 B. Suresh Kumar, P. Puthiaraj, A. J. Amali and K. Pitchumani, *ACS Sustainable Chem. Eng.*, 2018, **6**, 491–500.
15 P. Choudhary, A. Kumar, A. Bahuguna and V. Krishnan, in *Emerging Carbon Based Nanocomposites for Environmental Applications*, Wiley, 2020, ch. 4, pp. 71–119.
16 Z. Peng, Z. Wu, X. Sun and H. Li, *Green Chem.*, 2023, **25**, 6869–6880.
17 W. Zhang, M. Zhang, R. Wang, X. Guo and J.-H. Yang, *ChemistrySelect*, 2024, **9**, e202402396.
18 A. S. Rajpurohit, T. V. R. Mohan, M. Jaccob, K. K. Ramaswamy and B. Viswanathan, *ChemNanoMat*, 2023, **9**, e202300158.
19 S. Kumar, P. Choudhary, D. Sharma and V. Krishnan, *ChemNanoMat*, 2025, **11**, e202400564.
20 J. M. Guarinos, F. G. Cirujano, A. Rapeyko and F. X. Llabrés i Xamena, *Mol. Catal.*, 2021, **515**, 111925.
21 S. Varimalla, K. Manda, S. Boggala, R. C. Nappuni, S. Inkollu, H. P. Aytam and V. Akula, *Catal. Today*, 2024, **441**, 114916.
22 A. Patel and K. Chauhan, *Energy Fuels*, 2024, **38**, 15397–15409.
23 A. Patel and A. Patel, *RSC Adv.*, 2019, **9**, 1460–1471.
24 Y. Zhang, Y. Li, C. Shen, C. Yang, H. Wu, C. Jiang, S. Chen, M. Li, Y. Li, W. Ding and X. Guo, *Appl. Catal., B*, 2025, **361**, 124595.
25 A. M. Hengne, A. V. Malawadkar, N. S. Biradar and C. V. Rode, *RSC Adv.*, 2014, **4**, 9730–9736.
26 P. P. Upare, M.-G. Jeong, Y. K. Hwang, D. H. Kim, Y. D. Kim, D. W. Hwang, U.-H. Lee and J.-S. Chang, *Appl. Catal., A*, 2015, **491**, 127–135.
27 M. Varkolu, V. Velpula, D. R. Burri and S. R. R. Kamaraju, *New J. Chem.*, 2016, **40**, 3261–3267.
28 M. Varkolu, D. R. Burri, S. R. R. Kamaraju, S. B. Jonnalagadda and W. E. van Zyl, *Chem. Eng. Technol.*, 2017, **40**, 719–726.
29 S. Gundekari and K. Srinivasan, *Catal. Commun.*, 2017, **102**, 40–43.
30 S. Gundekari and K. Srinivasan, *Catal. Lett.*, 2019, **149**, 215–227.
31 K. Sakakibara, K. Endo and T. Osawa, *Catal. Commun.*, 2019, **125**, 52–55.
32 L. F. Sosa, V. T. da Silva and P. M. de Souza, *Catal. Today*, 2021, **381**, 86–95.
33 A. García, R. Sanchis, F. J. Llopis, I. Vázquez, M. P. Pico, M. L. López, I. Álvarez-Serrano and B. Solsona, *Energies*, 2020, **13**, 3448.
34 J. Patel and A. Patel, *Renewable Energy*, 2022, **201**, 190–201.
35 P. Hou, H. Su, K. Jin, Q. Li and W. Yan, *Molecules*, 2024, **29**, 3779.
36 R. Zhao and J. W. Bae, *Catal. Today*, 2024, **435**, 114718.
37 N. Yu, H. Lu, W. Yang, Y. Zheng, Q. Hu, Y. Liu, K. Wu and B. Liang, *Biomass Convers. Biorefin.*, 2024, **14**, 8271–8282.
38 S. Varimalla, K. Manda, S. Boggala, R. C. Nappuni, S. Inkollu, H. P. Aytam and V. Akula, *Catal. Today*, 2024, **441**, 114916.
39 M. Misono, *Mol. Eng.*, 1993, **3**, 193–203.
40 M. Khalid, M. Granollers Mesa, D. Scapens and A. Osatiashtiani, *ACS Sustainable Chem. Eng.*, 2024, **12**, 16494–16517.
41 D. Zhang, Y. Zhang, H. Li, Y. Zhang and P. Zhang, *ACS Sustainable Chem. Eng.*, 2025, **13**, 471–481.
42 A. Patel and M. Joshi, *Energy Fuels*, 2023, **37**, 9247–9256.
43 R. Le Van Mao, N. Al-Yassir, L. Lu, N. T. Vu and A. Fortier, *Catal. Lett.*, 2006, **112**, 13–18.
44 T. Okuhara, N. Mizuno and M. Misono, *Adv. Catal.*, 1996, **41**, 113–252.
45 J. Zhang, F. Tian, J. Chen, Y. Shi, H. Cao, P. Ning, S. Sun and Y. Xie, *Front. Chem. Sci. Eng.*, 2021, **15**, 288–298.
46 N. A. S. Ramli and N. A. S. Amin, *Appl. Catal., B*, 2015, **163**, 487–498.
47 A. Patel and M. Joshi, *Catal. Lett.*, 2024, **154**, 5887–5905.
48 Y. Peng and H. He, *RSC Adv.*, 2021, **11**, 39493–39502.
49 B. Laïk, M. Richet, N. Emery, S. Bach, L. Perrière, Y. Cotrebil, V. Russier, I. Guillot and P. Dubot, *ACS Omega*, 2024, **9**, 40707–40722.
50 J. Y. Son, S. H. Kim, J. M. Seo, J. Lim, T.-M. Chung and B. K. Park, *ACS Omega*, 2023, **8**, 19816–19821.
51 W. Cui, D. Zhu, J. Tan, N. Chen, D. Fan, J. Wang, J. Han, L. Wang, P. Tian and Z. Liu, *Chin. J. Catal.*, 2022, **43**, 1945–1954.
52 A. Chauhan, R. Bal and R. Srivastava, *Energy Fuels*, 2024, **38**, 5998–6011.
53 Y. Li, B. Liu, Y. Wang, S. Wang, X. Lan and T. Wang, *ACS Catal.*, 2022, **12**, 7926–7935.
54 G. C. Bond, *Heterogeneous Catalysis: Principles and Applications*, Clarendon Press, Oxford, 1974.
55 Z. Yang, Q. Ge and X. Zhu, *Green Chem.*, 2024, **26**, 8068–8099.
56 O. A. Petcuta, N. C. Guzo, M. Bordeiasu, A. Nicolaev, V. I. Parvulescu and S. M. Coman, *Catalysts*, 2025, **15**, 80.
57 O. Abdulhadi, I. Rahmman and A. S. Obaid, *J. Phys.: Conf. Ser.*, 2021, **2114**, 012083.
58 S. Rana, J. J. Velázquez and S. B. Jonnalagadda, *Nanoscale Adv.*, 2022, **4**, 3131–3135.
59 X. Tian, P. Yi, J. Sun, C. Li, R. Liu and J.-K. Sun, *Nanomaterials*, 2022, **12**, 1848.